

See discussions, stats, and author profiles for this publication at: <https://www.researchgate.net/publication/26771826>

Synthesis by AGET ATRP of Degradable Nanogel Precursors for In Situ Formation of Nanostructured Hyaluronic Acid Hydrogel

ARTICLE *in* BIOMACROMOLECULES · SEPTEMBER 2009

Impact Factor: 5.75 · DOI: 10.1021/bm9004639 · Source: PubMed

CITATIONS

48

READS

104

3 AUTHORS, INCLUDING:



[Sidi Bencherif](#)

Harvard University

36 PUBLICATIONS 1,478 CITATIONS

[SEE PROFILE](#)

Synthesis by AGET ATRP of Degradable Nanogel Precursors for In Situ Formation of Nanostructured Hyaluronic Acid Hydrogel

Sidi A. Bencherif,[†] Newell R. Washburn,^{†,‡} and Krzysztof Matyjaszewski*,[†]

Department of Chemistry and Department of Biomedical Engineering, Carnegie Mellon University, Pittsburgh, Pennsylvania 15213

Received April 23, 2009; Revised Manuscript Received July 4, 2009

A nanostructured hyaluronic acid (HA) hydrogel was prepared by a combination of atom transfer radical polymerization (ATRP) and Michael-type addition reaction. Biodegradable $\text{POEO}_{300}\text{MA}-co\text{-}\text{PHEMA}$ nanogels with pendent hydroxy groups were prepared by activators generated by electron transfer ATRP in cyclohexane inverse miniemulsion in the presence of a hydrolytically labile cross-linker. The hydroxy groups were subsequently modified with acryloyl chloride to form reactive acrylated-nanogels (ACRL-nanogels). These nanogels degrade upon hydrolysis into polymeric sols enabling controlled release of entrapped fluorescently labeled biomolecules, such as rhodamine B isothiocyanate-dextran used as a drug model. Thiol-derivatized HA (HA-SH) was prepared by carbodiimide-mediated coupling reaction of HA with cysteamine hydrochloride. The nanostructured hydrogel was formed by mixing HA-SH with ACRL-nanogels under physiological conditions ($\text{pH} = 7.4, 37^\circ\text{C}$). Gelation occurred within a few minutes after mixing the precursor liquid solution via a Michael-type addition reaction between unsaturated acrylated moieties and nucleophilic thiols, leading to a chemically cross-linked network. Formation of the nanostructured HA hydrogel was visually observed with digital images after gelation and hydration. The gel was analyzed by scanning electron microscopy for morphological observation. Surface morphology demonstrates that the nanostructured gel was well-constructed with a porous three-dimensional structure and uniform distribution of nanogels. This novel biodegradable scaffold hybridized with nanogels offers the advantage of selective, fast, *in situ* polymerization and potential as an injectable biocompatible matrix for cell and protein encapsulation in both tissue engineering and drug delivery applications.

Introduction

Hydrogels with new properties are being sought for a number of biomedical applications, including drug delivery matrices^{1–7} and tissue engineering scaffolds.^{8–15} Controlled drug delivery and its applications for tissue engineering for support and stimulation of tissue growth has attracted much attention over the past decade. The criteria for choosing materials to act as the foundation for a scaffold are challenging. The materials used must be safe, not cause excessive immune responses, possess acceptable biocompatibility, be nontoxic, and be eliminated in a controlled manner. The materials that combine such characteristics can be divided into three main categories: natural polymers including hyaluronic acid (HA),^{16–18} alginate,¹⁹ chitosan,²⁰ and proteins,^{21,22} synthetic polymers, mainly aliphatic polyesters,²³ and inorganic biomaterials, including hydroxyl apatite. Recently, HA-based hydrogels have generated interest in the biomaterials field as HA is naturally bioactive, biocompatible, resorbable, and angiogenic when degraded to small fragments upon enzymatic degradation.^{24–31}

Development of an *in situ* hydrogel has been recognized as a promising technology for biomedical applications.^{16,32–35} From the perspective of biomaterial administration to patients, the injection of a large implant hydrogel is possible via minimally invasive surgery and at the same time its *in situ* formation from a liquid precursor placed at the implantation

site can also match conformation of the final hydrogel implant to the irregular, complex tissue shapes.^{33,34} Another advantage of *in situ* hydrogels may be the easy encapsulation of cells in the matrix by mixing the cells in precursor liquids and then transforming the liquid solution into a cross-linked hydrogel network, thus confining the cells in a unique cross-linked mesh structure.³⁶ Furthermore, nutrients, wastes, and other important biomolecules could be freely transported to such a hydrogel, which is important in tissue engineering and cell therapy.³⁷

Different types of *in situ* hydrogels have been developed by employing various chemistries. Recent strategies have included modifying HA with cross-linkable moieties, namely, methacrylates,^{39,40} to enable hydrogel fabrication by photopolymerization mechanisms.^{17,23,25,28,38,40–43} In contrast to the employment of photokinetics in hydrogel synthesis, injectable matrices have been the subject of much research in the field of drug delivery. For example, HA has been modified with thiol side groups, which in the presence of air form a disulfide cross-link.⁴⁴ This mechanism was used to successfully encapsulate fibroblasts; however, the gelation process took several hours.⁴⁴ Alternatively, Michael-type addition reactions have been explored and have exhibited gelation times on the order of minutes.^{45–49} HA hydrogels have also been fabricated through this mechanism where either acrylated HA was reacted with PEG-tetrathiol⁵⁰ or thiol-modified HA was reacted with PEG diacrylate.^{46,51,52} One attractive feature of this type of cross-linking mechanism is that it requires no additional component, such as an initiator, and avoids the formation of nondegradable “kinetic chains”.⁴⁵

* To whom correspondence should be addressed. E-mail: km3b@andrew.cmu.edu. Phone: 412-268-3209. Fax: 412-268-6897.

[†] Department of Chemistry.

[‡] Department of Biomedical Engineering.

Hydrogels hybridized with nanosized particles have been increasingly explored in the design of new biomaterials with unique properties.⁵³ Recently, we reported the design of a new implantable nanostructured hydrogel via photopolymerization⁵⁴ for controlled release of multiple biomolecules, as is often required in the complex cascade of events involved in tissue regeneration. However, with a constant desire to improve the system, we were interested in designing a less invasive option where the nanostructured solidifiable precursors would self-cross-link upon injection without UV-irradiation.

This paper focuses on the synthesis of a new in situ biodegradable nanostructured HA hydrogel formed by mixing thiolated hyaluronic acid (HA-SH) with well-defined rhodamine B isothiocyanate-dextran (RITC-Dx) loaded acrylated-POEO₃₀₀-MA-*co*-PHEMA nanogels (ACRL-nanogels) prepared by activators generated by electron transfer (AGET) atom transfer radical polymerization (ATRP).^{55–60} The gelation of the pre-hydrogel solution occurs via a Michael-type addition reaction leading to a chemically cross-linked hybrid gel under physiological conditions ($\text{pH} = 7.4$, 37 °C). The network can be readily formed in direct contact with tissues, cells, and biological molecules and, thus, has utility as a scaffold for tissue engineering and as a delivery matrix for sensitive biologics. Both tissue engineering and drug delivery techniques can benefit from the use of this injectable material due to the injection being only minimally invasive, its ability to rapidly self-organize into a three-dimensional (3D) scaffold, and the presence of a nanoscale polymeric reservoir for controlled release of biomolecules. Because of these qualities, significant crossover should be observed for new nanostructured injectable materials in tissue engineering and drug delivery.

Experimental Section

Materials. OEO₃₀₀MA (300 g/mol, EO units ≈ 5) was purchased from Aldrich and purified by passing through a column filled with basic alumina to remove inhibitor. Poly(ethylene glycol) (PEG_{4k} ~ 4 × 10³ g/mol, DP_{PEG} ≈ 91), 2-hydroxyethyl methacrylate (HEMA), methacrylic anhydride (MA), acryloyl chloride (AC), *N*-hydroxybenzotriazole (HOBT), copper(II) bromide (CuBr₂), 4-dimethylaminopyridine (DMAP), phosphate-buffered saline (PBS), 1-ethyl-3-(3-dimethylaminopropyl)-carbodiimide (EDC), triethylamine (TEA), 4-hydroxy-2,2,6,6-tetramethylpiperidine-1-oxyl (hydroxy-TEMPO), ascorbic acid (AscA), and RITC-Dx (6 × 10⁴ g/mol) were purchased from Sigma-Aldrich and used as received. Tris[(2-pyridyl)-methyl]amine (TPMA) was purchased from ATRP Solutions, Inc. HA (3.5 × 10⁴ g/mol) was obtained from Lifecore Biomedical, Inc. Dichloromethane was purchased from Sigma-Aldrich and dried over activated molecular sieves (4 Å) prior to use. Glycolide was purchased from E. I. du Pont de Nemours. Poly(ethylene oxide)-functionalized 2-bromoisobutyrate (PEO_{2k}-Br ~ 2 × 10³ g/mol, DP_{PEO} ≈ 45) was synthesized as reported previously.⁶⁰ All other chemicals used were of reagent grade and were used without further purification.

Measurements. High-resolution, 300 MHz proton NMR spectra were taken on a Bruker Avance 300 spectrometer. Deuterium chloroform (CDCl₃) or deuterium oxide (D₂O) was used as solvent, and polymer concentrations were varied between 0.5 and 3% by mass fraction. All spectra were run at room temperature, 15 Hz sample spinning, 45° tip angle for the observation pulse, and a 10 s recycle delay, for 128 scans. The standard relative uncertainty for calculation of reaction conversion via ¹H NMR arises from the choice of baseline and is estimated to be 8%.

Molecular weight of degraded nanogels was determined by gel permeation chromatography (GPC; Polymer Standards Services (PSS) columns (guard, 10⁵, 10³, and 10² Å), with DMF eluent at 35 °C, flow rate = 1.00 mL/min, and differential refractive index (RI) detector

(Waters, 2410)). The apparent molecular weights and polydispersity (M_w/M_n) were determined with a calibration based on linear poly(methyl methacrylate) (polyMMA) standards using WinGPC 6.0 software from PSS.

Particle size and size distribution of nanogels were measured by dynamic light scattering (DLS) on High Performance Particle Sizer, Model HP5001 from Malvern Instruments, Ltd. DLS measurements provided the volume average diameter, D_{av} , and size distribution index, CV (coefficient of variation), which is defined as $CV = S/D_{av}$, where S is the size standard deviation.

Synthesis of PEG_{4k}-*co*-PGA DM. The degradable cross-linker was prepared as described previously.^{61,62} PEG_{4k}-*co*-PGA was prepared from the reaction of PEG_{4k} and glycolide at a ratio of 5 mol of glycolide/mol of PEG_{4k}. A total of 5 g of dry PEG_{4k}, 0.73 g of glycolide, and 2.5 mg of stannous octoate were charged into a 50 mL round-bottomed flask under a nitrogen atmosphere. The reaction mixture was stirred under vacuum at 200 °C for 4 h and at 160 °C for 2 h and subsequently cooled to room temperature. PEG_{4k}-*co*-PGA was dissolved in dichloromethane, precipitated in anhydrous ether, filtered, and dried in a vacuum oven overnight at room temperature.

PEG_{4k}-*co*-PGA DM was prepared from the reaction of PEG_{4k}-*co*-PGA with MA. PEG_{4k}-*co*-PGA (5 g, 1.1 mmol), 2.2 equiv of MA (0.37 g, 2.4 mmol), and TEA (0.2 mL) were reacted in 15 mL of dichloromethane over freshly activated molecular sieves (3 g) for 4 days at room temperature. The solution was precipitated twice into ethyl ether. The product was filtered and then dried in a vacuum oven overnight at room temperature.

Synthesis of Biodegradable POEO₃₀₀MA-*co*-PHEMA Nanogels by AGET ATRP. The synthesis of RITC-Dx-loaded POEO₃₀₀MA-*co*-PHEMA nanogels by inverse miniemulsion AGET ATRP in cyclohexane was according to the following ratio: [OEO₃₀₀MA]₀/[HEMA]₀/[PEO_{2k}-Br]₀/[CuBr₂/TPMA]₀/[AscA]₀/[PEG_{4k}-*co*-PGA DM] = 120/30/1/0.5/0.45/4.

A typical procedure for the synthesis is described below. OEO₃₀₀MA (2.51 g, 8.37 mmol), HEMA (0.27 g, 2.09 mmol), PEO_{2k}-Br (150 mg, 0.07 mmol), PEG_{4k}-*co*-PGA DM (1.23 g, 0.28 mmol), TPMA (10.1 mg, 0.035 mmol), CuBr₂ (0.0078 mg, 0.035 mmol), RITC-Dx (95 mg, 0.0014 mmol), and water (4.04 mL) were mixed in a 200 mL round-bottom flask at room temperature. The resulting clear solution was mixed with a solution of Span 80 (2.9 g) in cyclohexane (57.7 g), and the mixture was sonicated for 2 min in an ice bath at 0 °C to form a stable inverse miniemulsion. The dispersion was transferred into a 200 mL Schlenk flask and then bubbled with argon for 30 min. The flask was immersed in an oil bath preheated to 30 °C, and then an argon-purged 330 μL aqueous solution of AscA (5.5 mg, 0.03 mmol) was added via syringe to activate the catalyst and start the polymerization.

The polymerization was stopped after 17 h by exposing the reaction mixture to air. A stable pink dispersion was obtained. The cross-linked nanogels were purified by addition of THF to the resulting dispersion, and then the resulting heterogeneous mixture was stirred at room temperature for 30 min. The nanogels were separated by centrifugation at 13000 rpm for 30 min at 4 °C. After the supernatant was removed, THF was added, and then the same procedure was repeated twice to completely remove THF-soluble species including unreacted monomer and surfactant. The nanogels were resuspended in water, dialyzed against deionized water for 4 days using dialysis membrane with MWCO of 15000, and freeze-dried for 2 days (yield, 3.96 g).

Acrylation of POEO₃₀₀MA-*co*-PHEMA Nanogels. ACRL-nanogels were prepared from the reaction of hydroxy-containing nanogels with AC. HO-nanogels (320 mg, 250 μmol of hydroxy groups) were swollen in 15 mL of dimethylformamide (DMF) in a 50 mL round-bottomed flask and were cooled to 0 °C in an ice bath. A total of 202 mg (2 mmol) triethylamine (TEA) and 235 mg (2.50 mmol) AC in 5 mL of DMF was added to the flask upon stirring, and the reaction mixture was allowed to proceed for 12 h at 0 °C and for 12 h at room temperature. For the purification step, the reaction mixture was diluted in methanol to dissolve the TEA hydrochloride byproduct. ACRL-

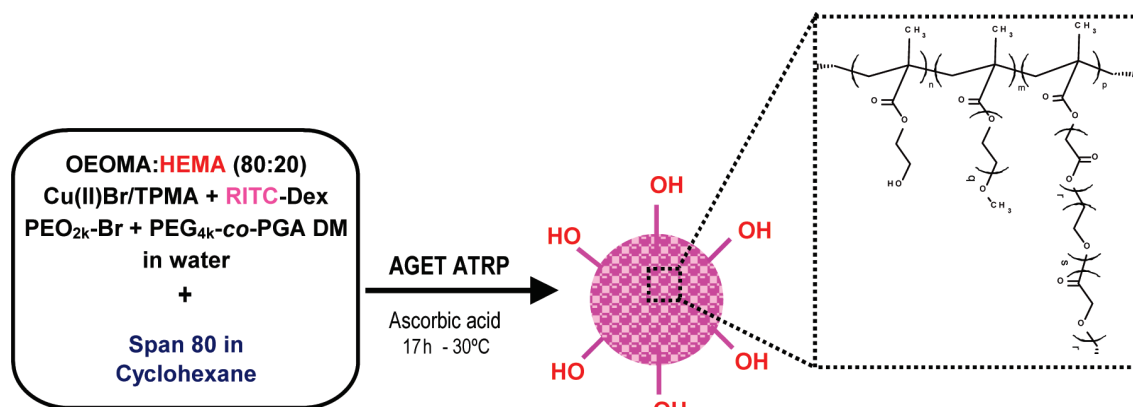


Figure 1. Synthesis of hydrolyzable RITC-Dx loaded $\text{POEO}_{300}\text{MA}$ -co-PHEMA nanogels by AGET ATRP in water-in-oil inverse miniemulsion polymerization, according to the following ratio: $[\text{OEO}_{300}\text{MA}]_0/[\text{HEMA}]_0/[\text{PEO}_{2k}\text{-Br}]_0/[\text{CuBr}_2/\text{TPMA}]_0/[\text{AscA}]_0/[\text{PEG}_{4k}\text{-co-PGADM}] = 120/30/1/0.5/0.45/4$.

nanogels were isolated by centrifugation and washed with methanol before being centrifuged again to remove the solvent. ACRL-nanogels were subsequently suspended in water, dialyzed against deionized water for 2 days using a dialysis membrane with a 15000 MWCO, and freeze-dried for 2 days. The resulting product was characterized by ^1H NMR.

Acid-Catalyzed Degradation of Nanogels. RITC-Dx loaded $\text{POEO}_{300}\text{MA}$ -co-PHEMA nanogels were dispersed in water (10 mg/mL) and HCl was subsequently added to a final pH ~ 2 . The solution was heated at 80 °C for 2 days to hydrolyze the ester bonds from degradable nanogels. The acidified solution was neutralized by adding dropwise a solution of sodium hydroxide (0.5 M NaOH) and freeze-dried for 1 day.

Synthesis of Thiol-Derivatized HA (HA-SH). HA was modified with thiol groups by using the reaction of carboxylic acid with cysteamine hydrochloride. HA (1.5 g, 3.7 mmol) was dissolved in deionized water (20 mL) and DMSO (10 mL). EDC (8 g, 37 mmol), HOBT (16 g, 111 mmol), 4-DMAP (0.3 g), and cysteamine hydrochloride (13.5 g, 111 mmol) were added as solids to the HA solution. The reaction proceeded at room temperature for 5 days. The byproduct was removed by filtration and the solution was precipitated twice in a large excess of methanol, filtered, and dried in a vacuum oven overnight at room temperature. The resulting product was characterized by ^1H NMR spectroscopy.

Preparation of Nanostructured HA Hydrogel. HA-SH (2 wt %) and ACRL- $\text{POEO}_{300}\text{MA}$ -co-PHEMA (5 wt %) nanogels were mixed in a phosphate-buffered saline solution at pH 7.4. The solution was rapidly transferred through a syringe into a mold to prepare cylindrical-shaped hydrogels. The mold was incubated up to 1 h at 37 °C to form a cross-linked network. The hydrogels were formed from the combination of the two reactive prehydrogel components (multifunctional thiolated HA and ACRL-nanogels) within 10 min under physiological conditions.

Microscopic Characterization of Hydrogel Surface Morphology. The nanostructured HA hydrogel was first equilibrated in PBS for 24 h at room temperature and then very quickly frozen below its freezing point using liquid nitrogen as cryogen. Cryofracturing of the frozen specimen was done to obtain a cross-section of the hydrogel interior that would reveal its structure. The frozen hydrogel was fractured with a sharp scalpel. The swollen freeze-dried sample was then mounted onto an aluminum stud and sputter-coated with a thin layer of gold (Dentin Vacuum Desc II) prior to imaging. Surface topographies of the freeze-dried swollen hydrogel specimen were investigated by a field emission scanning electron microscope (JEOL JSM 5400).

Results and Discussion

Synthesis and Characterization of ACRL- $\text{POEO}_{300}\text{MA}$ -co-PHEMA Nanogels. ATRP in inverse miniemulsion polymerization has been explored for the preparation of cross-linked

particles and gels with well-controlled polymer segments.^{56,57,63–66} This approach makes possible the preparation of biomaterials with many useful predetermined site specific features, including uniform network, high loading efficiency of biomolecules or drugs, distributed bromine end-group functionalities, and degradable microstructure.⁵⁷ Based on this method, we polymerized water-soluble $\text{OEO}_{300}\text{MA}$ macromonomer with pendent oligo(ethylene oxide) chain monomer in the presence of hydrolyzable PEG_{4k} -co-PGA DM cross-linker. $\text{OEO}_{300}\text{MA}$ is an analogue of linear poly(ethylene oxide), which is known to be biocompatible, to have low toxicity, and to prevent nanoparticle uptake by the reticularendothelial system.⁶⁷ The preparation of functionalized nanogels is required for further chemical modification (e.g., acylation). Our approach involved the introduction of a functional monomer, 2-hydroxyethyl methacrylate (HEMA, 25 mol % of $\text{OEO}_{300}\text{MA}$), as a comonomer in inverse miniemulsion AGET ATRP. This approach enabled preparation of functionalized $\text{POEO}_{300}\text{MA}$ -co-PHEMA nanogels with pendent hydroxy groups.

Synthesis of Degradable RITC-Dx Loaded $\text{POEO}_{300}\text{MA}$ -co-PHEMA Nanogels. As shown in Figure 1, well-controlled water-soluble RITC-Dx loaded $\text{POEO}_{300}\text{MA}$ -co-PHEMA nanogels functionalized with hydroxy groups were successfully prepared by AGET ATRP of $\text{OEO}_{300}\text{MA}$ and HEMA in the presence of $\text{PEO}_{2k}\text{-Br}$ initiator in inverse miniemulsion of water/cyclohexane at ambient temperature (30 °C) using Span 80 as an oil-soluble surfactant, TPMA/CuBr₂ as the catalyst precursor, PEG_{4k} -co-PGA DM as a hydrolyzable cross-linker, and AscA as a reducing agent. RITC-Dx was used not only to tag the nanogels, but also as an encapsulated drug model. During the polymerization, two methacrylate groups from PEG_{4k} -co-PGA DM provided gelation by rapid linking two growing chains, ultimately resulting in the formation of resorbable cross-linked nanogels.

Characterization of RITC-Dx Loaded $\text{POEO}_{300}\text{MA}$ -co-PHEMA Nanogels. RITC-Dx loaded $\text{POEO}_{300}\text{MA}$ -co-PHEMA nanogels were analyzed by ^1H NMR (Figure 2). The broadening of the peaks is a result of the high molecular weight of the cross-linked network. However, it is apparent from the identification of the peaks that $\text{POEO}_{300}\text{MA}$ -co-PHEMA nanogels were successfully formed via ATRP using PEG_{4k} -co-PGA DM cross-linker. Unreacted monomers were quantitatively removed during the purification step as no unreacted vinyl peaks from nanogels were observed in the range of 5.5–6.5 ppm. The assignment of resonance peaks in the spectrum, as shown in Figure 2, allows quantitative determination of both monomeric units ($\text{OEO}_{300}\text{MA}$ and HEMA) incorporated into the copolymers and the cross-

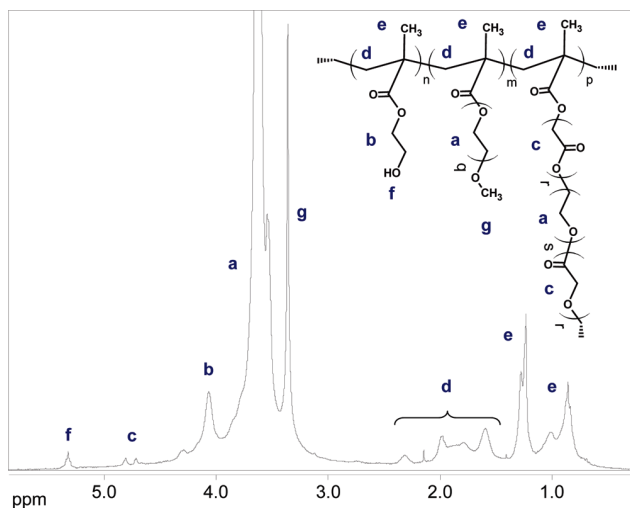


Figure 2. ^1H NMR (300 MHz) spectrum of $\text{POEO}_{300}\text{MA}-\text{co-PHEMA}$ nanogels in CDCl_3 . Each proton from PHEMA, $\text{POEO}_{300}\text{MA}$, and poly($\text{PEG}_{4k}\text{-co-PGA DM}$) was identified, confirming the formation of copolymer-based cross-linked nanogels. Repeat units q, r, and s were estimated to be 4.5, 3.4, and 90.5, respectively.

linker ($\text{PEG}_{4k}\text{-co-PGA DM}$) used to synthesize the nanogels. Thus, the mole ratio of $\text{OEO}_{300}\text{MA}$, HEMA, and poly($\text{PEG}_{4k}\text{-co-PGA DM}$) in the copolymer was determined from the integrated peak areas of the methoxy protons ($\delta_g \sim 3.3$ ppm) from $\text{POEO}_{300}\text{MA}$, hydroxy protons ($\delta_f \sim 5.2$ ppm) from PHEMA, and methylene protons ($\delta_c \sim 4.8\text{--}4.9$ ppm) from PGA extensions in the cross-linked block copolymer. The complex pattern of e and d peaks can arise from different chemical composition and also polymer tacticity. The random copolymerization of $\text{OEO}_{300}\text{MA}$, HEMA, and $\text{PEG}_{4k}\text{-co-PGA DM}$ was studied for the following feed composition [$\text{OEO}_{300}\text{MA}$]/[HEMA]/[$\text{PEG}_{4k}\text{-co-PGA DM}$] = 1:0.250:0.033. After the copolymerization the mole ratio of the monomers and cross-linker was calculated by measuring the integrated peak areas of g, f, and c, respectively, as follows: [$\text{OEO}_{300}\text{MA}$]/[HEMA]/[$\text{PEG}_{4k}\text{-co-PGA DM}$] = 1:0.234:0.029. Relative to the $\text{OEO}_{300}\text{MA}$ monomer, the copolymerization conversion of HEMA and $\text{PEG}_{4k}\text{-co-PGA DM}$ was 94 and 88%, respectively. Incomplete monomer and cross-linker conversions were obtained in our reaction conditions. However, unreacted monomers and cross-linker were quantitatively removed from the nanogels during the dialysis step as no vinyl groups were observed in the NMR spectrum. From the conversion of HEMA and $\text{PEG}_{4k}\text{-co-PGA DM}$, relative to $\text{OEO}_{300}\text{MA}$, the degrees of polymerization of the copolymers were estimated to be 34, 8, and 1, respectively, between two cross-link points.

Characterization of Size of the Nanogels Before and After Purification. The volume average size of nanogels was determined by DLS. As shown in Figure 3, the volume average size of the nanogels was $D_{av} = 203$ nm after purification. The nanogels were dispersed in deionized water after dialysis.

From the visual examinations and DLS characterization, the incorporation of PHEMA into the preparation of nanogels significantly reduced the self-aggregation of nanogels when compared to pure $\text{POEO}_{300}\text{MA}$ nanogels. The $\text{POEO}_{300}\text{MA}-\text{co-PHEMA}$ nanogels were more homogeneously dispersed and stable in water over a long period of time (several days) without aggregation.

Acrylation of $\text{POEO}_{300}\text{MA}-\text{co-PHEMA}$ Nanogels. As shown in Figure 4, a set of nanogels with pendent hydroxy groups was chemically modified with acryloyl chloride to functionalize the

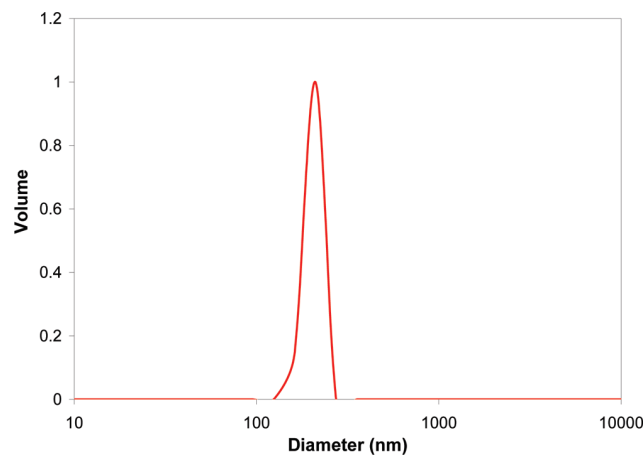


Figure 3. Characterization of the volume average size (diameter) by DLS of RITC-Dx loaded $\text{POEO}_{300}\text{MA}-\text{co-PHEMA}$ nanogels prepared by AGET ATRP immediately after dialysis and freeze-drying (size = 203 nm, CV = 0.48, in deionized water).

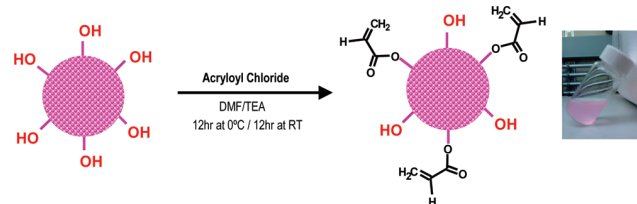


Figure 4. Acrylation of hydroxy-containing $\text{POEO}_{300}\text{MA}-\text{co-PHEMA}$ nanogels (ACRL-nanogels). HO-TEMPO was used after synthesis to prevent spontaneous free radical polymerization. Image shows dispersed ACRL-nanogels in water after purification with no evidence of intermolecular cross-linking.

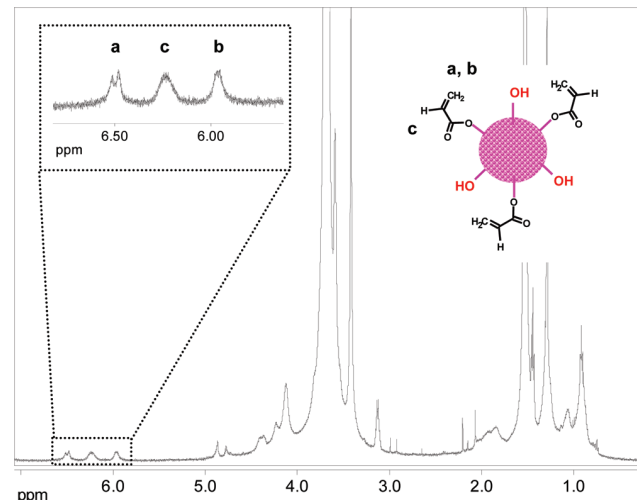


Figure 5. ^1H NMR (300 MHz) spectrum of ACRL- $\text{POEO}_{300}\text{MA}-\text{co-PHEMA}$ nanogels in CDCl_3 . Acrylate protons (a, b, and c) confirm the formation of ACRL-nanogels.

particle surface with acrylate groups for a further Michael-type addition reaction with thiomers.

Acrylation of hydroxy-containing nanogels with acryloyl chloride was confirmed by ^1H NMR spectroscopy as shown in Figure 5. Complete conversion of alcohol groups from nanogels into acrylates was supported by the disappearance of hydroxy peaks at 5.2 ppm (Figure 2), and appearance of three acrylate peaks (b, c, and a) at $\delta_b \sim 5.9$ ppm, $\delta_c \sim 6.2$ ppm, and $\delta_a \sim 6.5$ ppm, respectively (Figure 5). Furthermore, the appearance of the new acrylate peaks (as assessed via integration of NMR)

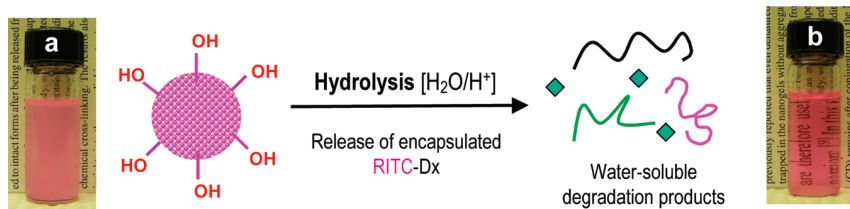


Figure 6. Acid-catalyzed hydrolysis of nanogels. Digital images of RITC-Dx loaded $\text{POEO}_{300}\text{MA}-\text{co-PHEMA}$ nanogels in water before (a) and after (b) degradation. Disappearance of the turbid suspension and formation of the corresponding transparent pink solution suggests nanogel degradation and release of encapsulated RITC-Dx.

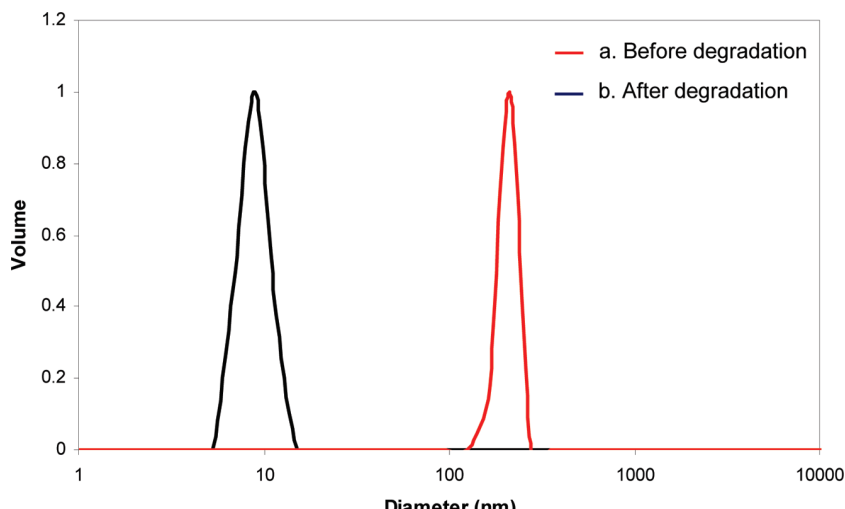


Figure 7. Characterization of nanogel size (volume average diameter) by DLS in deionized water before (a: size = 203 nm, CV = 0.48) and after acid-catalyzed hydrolysis (b: size = 9 nm, CV = 0.44).

matches the expected number of acrylates after all hydroxyl groups have reacted.

To avoid undesirable cross-linking during the freeze-drying process, hydroxy-TEMPO was used as a radical inhibitor at a concentration of 0.2 mg/mL. Hydroxy-TEMPO acts as a radical scavenger of free radicals. ACRL-nanogels spontaneously polymerize and form macroscopic cross-linked gels in the absence of radical traps.

Degradation of $\text{POEO}_{300}\text{MA}-\text{co-PHEMA}$ Nanogels. During the preparation of RITC-Dx loaded $\text{POEO}_{300}\text{MA}-\text{co-PHEMA}$ nanogels, $\text{PEG}_{4k}\text{-co-}\text{PGA}$ DM macromonomer was used as a cross-linker to form biodegradable cross-linked nanogels. The $\text{PEG}_{4k}\text{-co-}\text{PGA}$ backbone consists of hydrolytically labile ester bonds. It has previously been shown that the degradation of such polyester occurs via the cleavage of the ester bonds under physiological conditions.^{61,62} As the glycolide linkages are hydrolyzed and the cross-links are continually broken, a point is reached where the remaining polymer chains no longer combine to form a gel with an infinite weight-average molecular mass. When a sufficient number of cross-links have been broken, all that remains of the 3D nanosized network are separate polymer chains. Their dissolution into the surrounding media results in release of entrapped biomolecules (e.g., RITC-Dx). As shown in Figure 6, RITC-Dx loaded $\text{POEO}_{300}\text{MA}-\text{co-PHEMA}$ nanogels were degraded in water through the acid-catalyzed hydrolysis mechanism. The solution was heated at 80 °C for 2 days to ensure full hydrolysis of ester bonds from nanogels.

The nanogels degraded upon hydrolysis of the oligo(α -hydroxy acid) regions into water-soluble components: $\text{POEO}_{300}\text{MA}-\text{co-PHEMA}$, PEG_{4k} , PEO_{2k} , α -hydroxy acid, and acidic oligomers. The degradation of the nanogels was confirmed by

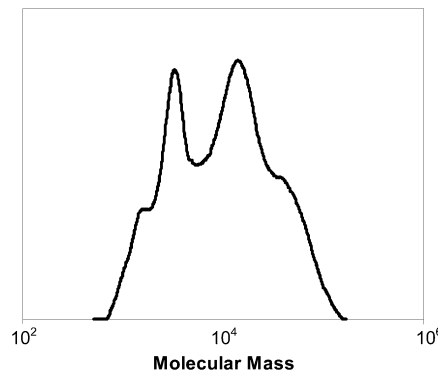
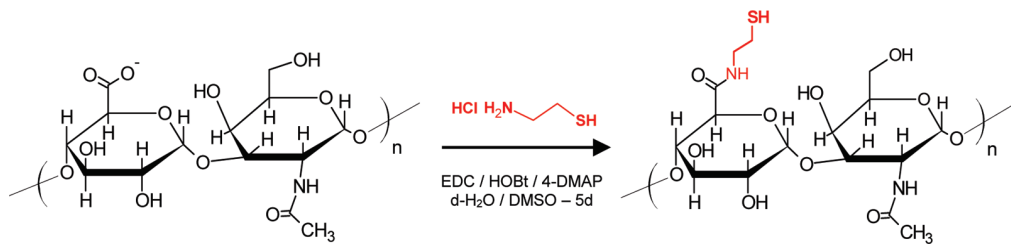


Figure 8. GPC profile of degraded $\text{POEO}_{300}\text{MA}-\text{co-PHEMA}$ nanogels ($M_n = 5.2 \times 10^3$, $M_w/M_n = 3.42$). The resulting degraded nanogels displayed a multimodal GPC trace, thus indicating a mixture of polymers presumably from PEO_{2k} -macroinitiator, PEG_{4k} central block from cross-linker, and $\text{POEO}_{300}\text{MA}-\text{co-PHEMA}$ statistical copolymer.

DLS characterization. As shown in Figure 7, the diameter of the particles decreased from 203 to 9 nm, corresponding to the size of polymeric sols after degradation.

The molecular weights of degraded polymers were determined by gel permeation chromatography. As shown in Figure 8, multimodal GPC trace was observed with an average M_n of degraded polymers of 5.2×10^3 g/mol with a broad molecular weight distribution of $M_w/M_n = 3.42$. The high polydispersity and multimodal profile comprising different components suggest that several polymers from the hydrolytic degradation of nanogels are combined in the degraded mixture. Two component peaks detected at the lowest molecular weight could be as PEO_{2k} from macroinitiator and PEG_{4k} central block from cross-linker. The

**Figure 9.** Synthesis of thiol-derivatized HA (HA-SH).

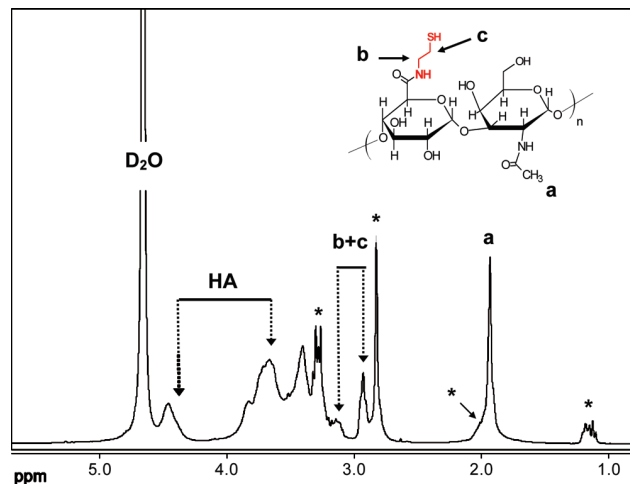
main peak at the highest molecular weight was assigned to POEO₃₀₀MA-*co*-PHEMA statistical block copolymer. The experimental molecular weight ($M_n \sim 39 \times 10^3$) for the statistical block copolymer is consistent with the targeted DP_{POEO300MA-*co*-PHEMA} (DP_{POEO300MA} = 120, DP_{PHEMA} = 30) and targeted molecular weight (MW_{POEO300MA-*co*-PHEMA} \approx DP_{POEO300MA} \times MW_{POEO300MA} + DP_{PHEMA} \times MW_{PHEMA} = 120 \times 300 + 30 \times 130 \approx 40 \times 10³), thus confirming that the polymerization was carried out in a controlled fashion with high conversions. A shoulder at the highest molecular weight could be ascribed to some aggregates or to incompletely degraded nanogels. Nevertheless, after degradation, the nanogels broke down into water-soluble polymer fragments with relatively small molecular weights, allowing possible excretion from the body via renal filtration in an *in vivo* application.

Release of RITC-Dx from cross-linked nanogels requires cleavage of a sufficient number of bonds to provide a pathway through the gel. As a consequence, the turbid solution of RITC-Dx containing nanogels dispersed in water (Figure 6a) turned to a transparent solution (Figure 6b). These results suggest that these biodegradable nanogels could be used as delivery carriers because biomolecules such as carbohydrate drugs or proteins can be released upon hydrolysis.

Synthesis of Thiolated HA. HA-SH conjugate was synthesized by amide bond formation between carboxylic acid groups of hyaluronic acid and amine groups of cysteamine. The reactivity of the thiol group toward Michael-type addition depends on the pK_a of the thiol group, because the thiolate anion is the actual reactive species in the Michael-type addition reaction. Therefore, the selection of cysteamine ligand was based upon its thiol pK_a value (8.3), which is higher than the physiological pH value (7.4) and lead to the formation of nucleophilic thiolate anion. As shown in Figure 9, cysteamine hydrochloride was covalently attached to hyaluronic acid mediated by carbodiimide and HOBT and introduced thiol groups into the polysaccharide backbone.

Structure of thiol-derivatized HA was confirmed by ¹H NMR (D₂O): δ_{b+c} 2.9–3.2 (m, 4H, CH₂CH₂; Figure 10). The conjugation was achieved with a high degree of functionalization as a large molar excess of cysteamine was used. The apparent degree of modification of HA with thiol groups was approximately 64 ± 2% (defined as the number of substituents per 100 repeat units).

Nanostructured Hydrogel via Michael-Type Addition Polymerization. A Michael addition reaction offers the possibility of obtaining *in situ* formation of polymeric hydrogels in the absence of a radical mechanism for the networking process. We explored such a synthetic route for obtaining a nanostructured HA hydrogel as a potential biomaterial by employing both water-soluble acrylated POEO₃₀₀MA-*co*-PHEMA nanogels and functionalized HA with multithiol end groups. The mechanism for Michael-type addition is base-catalyzed, which causes a step growth reaction between thiolate anions and acrylate functional groups under physiological conditions. The gel concentration was defined as the total dry weight of both HA-SH (2% wt) and ACRL-nanogels (5% wt) per volume of buffer. As shown

**Figure 10.** ¹H NMR (300 MHz) spectrum of thiolated HA (HA-SH) in D₂O. Chemical shift impurities from 1-ethyl-3-(3-dimethylaminopropyl)urea (EDU) in the course of amide coupling reaction are represented with the symbol *.

in Figure 11, before hydrogel formation, the solutions of the ACRL-nanogels and HA-SH were fluid. After mixing both reaction solutions, a cross-linked hydrogel was formed within a few minutes in a Teflon mold containing cylindrical-shaped holes of 5 mm in diameter and 5 mm in length. Gelation began within 10 min, right after mixing of both acrylated-nanogels and HA with thiol functional groups. The gel formation was determined by the vial tilting method.

One consequence of using Michael-type addition chemistry to form the cross-linked network was that thioethers were formed with thioester bonds within every cross-link (Figure 11). When the formed hydrogel was removed from the mold, the nanostructured hydrogel initially demonstrated a slight champagne-pink color in air but was translucent pink in water due to entrapped RITC-Dx. The hydrogel predefined by the employed mold swelled in PBS and its cylindrical form remained when in water.

For the scaffold to be used as a carrier for cells and sensitive compounds, the solidification process after injection should occur under physiological conditions. The gelation of the *in situ* nanostructured hydrogels occurs via Michael-type addition reaction within a few minutes leading to chemically cross-linked hybrid hydrogels under mild conditions (pH = 7.4, 37 °C). The Michael-type addition of thiols to the acryloyl derivative offers an interesting route for networking functionalized polymer chains without using a photocross-linking process. As shown in Figure 11, HA-based nanostructured hybrid hydrogel was obtained by the nucleophilic thiol-ene addition between the thiol-functionalized HA chains and the vinyl moieties contained in grafted acrylic nanogels. The gels generated by this method are well controlled, because no new polymeric species are formed.

The nanogels offer the advantage of having a second delivery carrier in addition to the 3D macroscopic scaffold for the

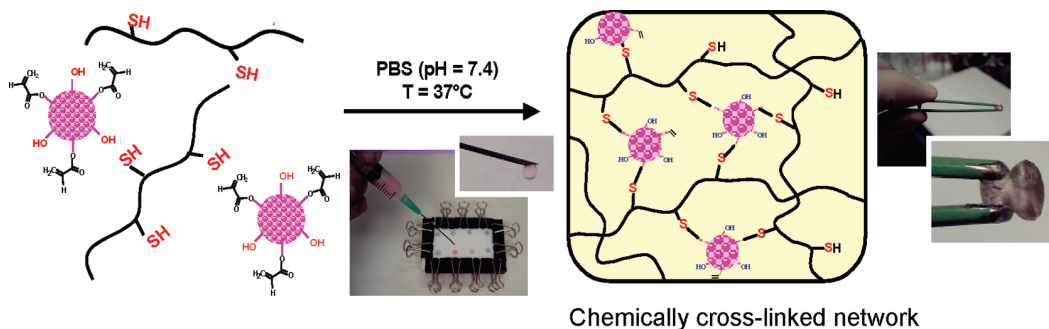


Figure 11. Gel formation via Michael-type addition reaction under physiological conditions. Formation of the nanostructured hybrid hydrogel was visually observed with digital images before and after gelation.

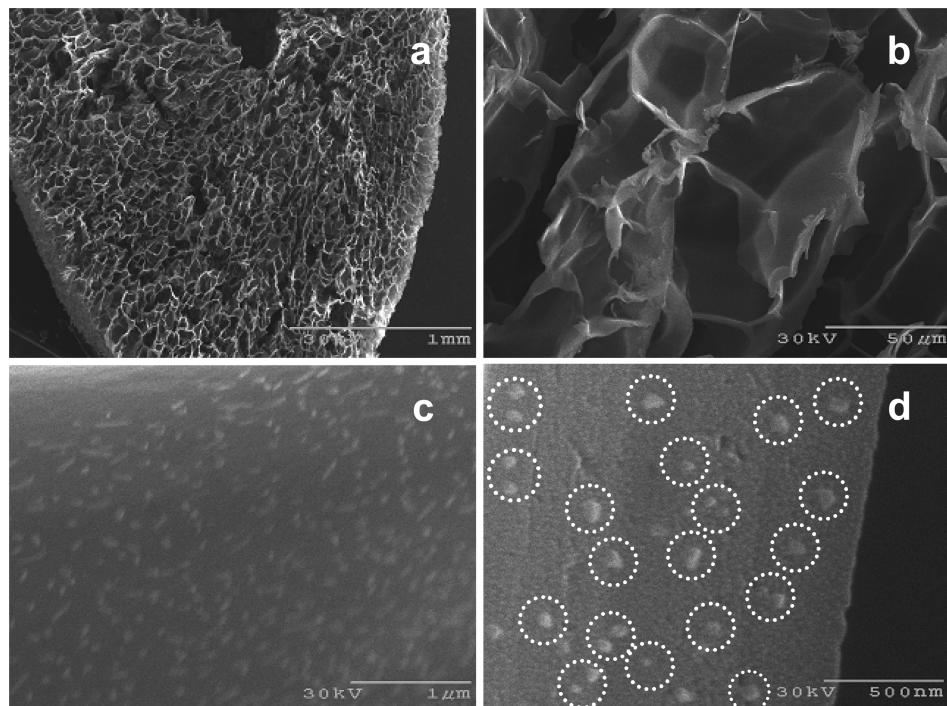


Figure 12. SEM photomicrographs of nanostructured HA hydrogel. Morphology and structure of SEM images: (a) overall image, (b) cross-section of interior, and surface hybridized with nanogels (c,d) at different magnifications. Dashed circles (d) denote nanogels homogeneously dispersed in the macroscopic HA hydrogel. The images are shown at the following scales: 1 mm (a), 50 μ m (b), 1 μ m (c), and 500 nm (d).

controlled delivery of smaller bioactive molecules. We previously reported that these nanogels could be used as delivery carriers and have potential to efficiently transfect cells when modified with a RGD cell adhesion sequence to potentially deliver entrapped biomolecules and drugs.⁶⁸ In our system, a biomimetic nanostructured scaffold can easily be obtained by incorporation of thiol-containing bioactive molecules, such as proteins and peptides.

Morphological Microstructure of Nanostructured HA Hydrogel. Characterization by scanning electron microscopy (SEM) of surface morphology was used to obtain insight into the 3D structure of the composite hydrogel. Surface microstructures of the hydrogel in swollen state were studied as shown in Figure 12.

The SEM study of the interior morphology of the swollen hydrogel clearly showed its 3D network structure. The structure observed by SEM should have very close to the original morphology without artifacts because the gel volume shrank by less than 1% after freeze-drying. This assumption is also supported by Hong and Chen's study of freeze-dried PVC/dioxane gels.⁶⁹

One parameter that must be considered in the design of a tissue-engineering scaffold is porosity. Void space is necessary within the scaffold network to allow for tissue growth, and diffusion of nutrients and waste products. In addition to total porosity, pore size and interconnectivity are also important. As shown in Figure 12b, the cross-sectional interior of the swollen hydrogel exhibits a rugged and highly porous honeycomb-like structure. The pores have assumed an irregular shape with their long axis less than 0.1 mm thick. The thickness of the pore wall is less than 3 μ m. The morphology and size of the pore structure observed are expected to be at the maximum limit that the nanostructured HA hydrogel can reach under this specific swelling condition (i.e., where gel reached equilibrium swelling within 2 h).

At a higher magnification (Figures 12c,d), the surface shows very tiny nanosized spheres. This result suggests that nanogels are part of the cross-linked scaffold and are homogeneously distributed as observed on the surface and in the interior structure of the nanostructured hydrogel. HA polymers combined with nanogels resulted in injectable composites with large porosity and the ability to incorporate drugs and growth factors. However,

this system may be easily adapted to enable controlled release of encapsulated drugs and growth factor from nanogels within the matrix.

Conclusion

We report on the synthesis of well-defined and functionalized degradable nanogel-precursors by AGET ATRP. The nanogels degraded upon hydrolysis of the oligo(α -hydroxy acid) regions from cross-linker into water-soluble polymers enabling controlled release of encapsulated RITC-Dx. POEO₃₀₀MA-*co*-PHEMA nanogels were subsequently modified with AC to form reactive ACRL-nanogel-precursors for *in situ* preparation of a novel nanostructured HA-based hydrogel. A complementary prehydrogel component, thiolated HA, was synthesized with a relatively high conversion and degree of purity. Nanostructured HA-based hydrogel was prepared within 10 min from the combination of the two reactive precursors (ACRL-nanogels and HA-SH) under physiological conditions ($pH = 7.4$, 37°C). Evaluation of gel morphology by SEM showed a porous 3D network structure with homogeneous distribution of nanogels. An extent of kinetic gel formation, water swelling, mechanical strength against compression, and biological activities of nanostructured HA-based hydrogels are under investigation.

The design of an injectable scaffold based on HA and nanogels shows promise in the fields of drug delivery and tissue engineering. Our degradable hyaluronic acid hydrogel provides a potential scaffold for tissue growth and matrix cell encapsulation, while the nanogels offer the advantage of having a second delivery carrier in addition to the macroscopic matrix for the controlled release of small biomolecules. This new type of nanostructured hydrogel is promising for use in biomedical applications, because it can be rapidly formed *in situ* and is biodegradable with the ability to control and target drug release from the matrix.

Acknowledgment. The members of the CRP Consortium at Carnegie Mellon University are gratefully acknowledged. Financial support was provided from NSF DMR 05-49353 (K.M.).

References and Notes

- Davis, K. A.; Quick, D. J.; Anseth, K. S. *Abstracts of Papers*, 224th National Meeting of the American Chemical Society, Boston, MA, Aug 18–22, 2002; American Chemical Society: Washington, DC, 2002; p U52.
- Lu, S. X.; Anseth, K. S. *Macromolecules* **2000**, *33*, 2509–2515.
- Langer, R.; Peppas, N. A. *AIChE J.* **2003**, *49*, 2990–3006.
- Kim, B.; Peppas, N. A. *Int. J. Pharm.* **2003**, *266*, 29–37.
- Langer, R.; Tirrell, D. A. *Nature* **2004**, *428*, 487–492.
- Hubbell, J. A. *Curr. Opin. Solid State Mater. Sci.* **1998**, *3*, 246–251.
- Peppas, N. A.; Merrill, E. W. *J. Biomed. Mater. Res.* **1977**, *11*, 423–434.
- Drury, J. L.; Mooney, D. J. *Biomaterials* **2003**, *24*, 4337–4351.
- Lee, K. Y.; Mooney, D. J. *Chem. Rev.* **2001**, *101*, 1869–1879.
- Koh, W. G.; Revzin, A.; Pishko, M. V. *Langmuir* **2002**, *18*, 2459–2462.
- Lutolf, M. P.; Lauer-Fields, J. L.; Schmoekel, H. G.; Metters, A. T.; Weber, F. E.; Fields, G. B.; Hubbell, J. A. *Proc. Natl. Acad. Sci. U.S.A.* **2003**, *100*, 5413–5418.
- Nguyen, K. T.; West, J. L. *Biomaterials* **2002**, *23*, 4307–4314.
- Schmedlen, K. H.; Masters, K. S.; West, J. L. *Biomaterials* **2002**, *23*, 4325–4332.
- Pratt, A. B.; Weber, F. E.; Schmoekel, H. G.; Muller, R.; Hubbell, J. A. *Biotechnol. Bioeng.* **2004**, *86*, 27–36.
- (a) Karp, J. M.; Dalton, P. D.; Shoichet, M. S. *MRS Bull.* **2003**, *28*, 301–306. (b) Dandu, R.; Ghandehari, H. *Prog. Polym. Sci.* **2007**, *32*, 1008–1030. (c) Goddard, J. M.; Hotchkiss, J. H. *Prog. Polym. Sci.* **2007**, *32*, 698–725. (d) Hoffman, A. S.; Stayton, P. S. *Prog. Polym. Sci.* **2007**, *32*, 922–932. (e) Kabanov, A. V.; Gendelman, H. E. *Prog. Polym. Sci.* **2007**, *32*, 1054–1082. (f) Nair, L. S.; Laurencin, C. T. *Prog. Polym. Sci.* **2007**, *32*, 762–798. (g) Pasut, G.; Veronese, F. M. *Prog. Polym. Sci.* **2007**, *32*, 933–961. (h) Rapoport, N. *Prog. Polym. Sci.* **2007**, *32*, 962–990. (i) Vert, M. *Prog. Polym. Sci.* **2007**, *32*, 755–761. (j) Wong, S. Y.; Pelet, J. M.; Putnam, D. *Prog. Polym. Sci.* **2007**, *32*, 799–837. (k) Yamato, M.; Akiyama, Y.; Kobayashi, J.; Yang, J.; Kikuchi, A.; Okano, T. *Prog. Polym. Sci.* **2007**, *32*, 1123–1133. (l) Bajpai, A. K.; Shukla, S. K.; Bhanu, S.; Kankane, S. *Prog. Polym. Sci.* **2008**, *33*, 1088–1118. (m) Kim, M. S.; Khang, G.; Lee, H. B. *Prog. Polym. Sci.* **2008**, *33*, 138–164. (n) Lutz, J.-F.; Boerner, H. G. *Prog. Polym. Sci.* **2008**, *33*, 1–39. (o) Park, J. H.; Lee, S.; Kim, J.-H.; Park, K.; Kim, K.; Kwon, I. C. *Prog. Polym. Sci.* **2008**, *33*, 113–137. (p) Venkatraman, S.; Boey, F.; Lao, L. L. *Prog. Polym. Sci.* **2008**, *33*, 853–874.
- Kim, G.-W.; Choi, Y.-J.; Kim, M.-S.; Park, Y.; Lee, K.-B.; Kim, I.-S.; Hwang, S.-J.; Noh, I. *Current Applied Physics*, 3rd China–Korea Symposium on Biomaterials and Nano-Bio Technology, 2007, *7*, e28–e32.
- Bencherif, S. A.; Srinivasan, A.; Horkay, F.; Hollinger, J. O.; Matyjaszewski, K.; Washburn, N. R. *Biomaterials* **2008**, *29*, 1739–1749.
- Shu, X. Z.; Ghosh, K.; Liu, Y.; Palumbo, F. S.; Luo, Y.; Clark, R. A.; Prestwich, G. D. *J. Biomed. Mater. Res., Part A* **2004**, *68*, 365–375.
- Hauselmann, H. J.; Aydelotte, M. B.; Schumacher, B. L.; Kuettner, K. E.; Gitelis, S. H.; Thonar, E. J. *Matrix* **1992**, *12*, 116–129.
- Kafedjiiski, K.; Krauland, A. H.; Hoffer, M. H.; Bernkop-Schnurch, A. *Biomaterials* **2005**, *26*, 819–826.
- Kimura, T.; Yasui, N.; Ohsawa, S.; Ono, K. *Clin. Orthop. Relat. Res.* **1984**, 231–239.
- Fortier, L. A.; Nixon, A. J.; Mohammed, H. O.; Lust, G. *Am. J. Vet. Res.* **1997**, *58*, 66–70.
- Bryant, S. J.; Anseth, K. S. *J. Biomed. Mater. Res.* **2002**, *59*, 63–72.
- Brekke, J. H.; Thacker, K. *Hyaluronan as a Biomaterial*; CRC Press: Boca Raton, FL, 2005.
- Burdick, J. A.; Chung, C.; Jia, X.; Randolph, M. A.; Langer, R. *Biomacromolecules* **2005**, *6*, 386–391.
- Chen, W. Y.; Abatangelo, G. *Wound Repair Regen.* **1999**, *7*, 79–89.
- Gupta, P.; Vermani, K.; Garg, S. *Drug Discovery Today* **2002**, *7*, 569–579.
- Leach, J. B.; Bivens, K. A.; Patrick, C. W.; Schmidt, C. E. *Biotechnol. Bioeng.* **2003**, *82*, 578–589.
- Luo, Y.; Ziebell, M. R.; Prestwich, G. D. *Biomacromolecules* **2000**, *1*, 208–218.
- Mengher, L. S.; Pandher, K. S.; Bron, A. J.; Davey, C. C. *Br. J. Ophthalmol.* **1986**, *70*, 442–447.
- Jia, X.; Burdick, J. A.; Kobler, J.; Clifton, R. J.; Rosowski, J. J.; Zeitels, S. M.; Langer, R. *Macromolecules* **2004**, *37*, 3239–3248.
- Heggli, M.; Tirelli, N.; Zisch, A.; Hubbell, J. A. *Bioconjugate Chem.* **2003**, *14*, 967–973.
- Brittberg, M.; Lindahl, A.; Nilsson, A.; Ohlsson, C.; Isaksson, O.; Peterson, L. *N. Engl. J. Med.* **1994**, *331*, 889–895.
- Grande, D. A.; Pitman, M. I.; Peterson, L.; Menche, D.; Klein, M. *J. Orthopaed. Res.* **1989**, *7*, 208–218.
- Martin, T. M.; Benguzzi, H.; Tucci, M. *Biomed. Sci. Instrum.* **2006**, *42*, 332–337.
- Lutolf, M. P.; Tirelli, N.; Cerritelli, S.; Cavalli, L.; Hubbell, J. A. *Bioconjugate. Chem.* **2001**, *12*, 1051–1056.
- Jen, A. C.; Wake, M. C.; Mikos, A. G. *Biotechnol. Bioeng.* **1996**, *50*, 357–364.
- Smeds, K. A.; Grinstaff, M. W. *J. Biomed. Mater. Res.* **2001**, *55*, 254–255.
- Masters, K. S.; Shah, D. N.; Leinwand, L. A.; Anseth, K. S. *Biomaterials* **2005**, *26*, 2517–2525.
- Chung, C.; Mesa, J.; Randolph, M. A.; Yaremchuk, M.; Burdick, J. A. *J. Biomed. Mater. Res., Part A* **2006**, *77A*, 518–525.
- Mann, B. K.; Gobin, A. S.; Tsai, A. T.; Schmedlen, R. H.; West, J. L. *Biomaterials* **2001**, *22*, 3045–3051.
- Cruise, G. M.; Scharp, D. S.; Hubbell, J. A. *Biomaterials* **1998**, *19*, 1287–1294.
- Rydholm, A. E.; Held, N. L.; Benoit, D. S. W.; Bowman, C. N.; Anseth, K. S. *J. Biomed. Mater. Res., Part A* **2008**, *86A*, 23–30.
- Shu, X. Z.; Liu, Y. C.; Luo, Y.; Roberts, M. C.; Prestwich, G. D. *Biomacromolecules* **2002**, *3*, 1304–1311.
- Park, Y.; Lutolf, M. P.; Hubbell, J. A.; Hunziker, E. B.; Wong, M. *Tissue Eng.* **2004**, *10*, 515–522.
- Shu, X. Z.; Liu, Y. C.; Palumbo, F. S.; Lu, Y.; Prestwich, G. D. *Biomaterials* **2004**, *25*, 1339–1348.
- Lutolf, M. P.; Hubbell, J. A. *Biomacromolecules* **2003**, *4*, 713–722.

- (48) Peattie, R. A.; Rieke, E. R.; Hewett, E. M.; Fisher, R. J.; Shu, X. Z.; Prestwich, G. D. *Biomaterials* **2006**, *27*, 1868–1875.
- (49) Hiemstra, C.; van der Aa, L. J.; Zhong, Z. Y.; Dijkstra, P. J.; Feijen, J. *Biomacromolecules* **2007**, *8*, 1548–1556.
- (50) Kim, J.; Kim, I. S.; Cho, T. H.; Lee, K. B.; Hwang, S. J.; Tae, G.; Noh, I.; Lee, S. H.; Park, Y.; Sun, K. *Biomaterials* **2007**, *28*, 1830–1837.
- (51) Shu, X. Z.; Ahmad, S.; Liu, Y. C.; Prestwich, G. D. *J. Biomed. Mater. Res., Part A* **2006**, *79A*, 902–912.
- (52) Flynn, L.; Prestwich, G. D.; Semple, J. L.; Woodhouse, K. A. *Biomaterials* **2007**, *28*, 3834–3842.
- (53) Richardson, T. P.; Peters, M. C.; Ennett, A. B.; Mooney, D. J. *Nat. Biotechnol.* **2001**, *19*, 1029–1034.
- (54) Bencherif, S. A.; Siegwart, D. J.; Srinivasan, A.; Horkay, F.; Hollinger, J. O.; Washburn, N. R.; Matyjaszewski, K. *Biomaterials* **2009**, *30*, 5270–5278.
- (55) (a) Wang, J. S.; Matyjaszewski, K. *J. Am. Chem. Soc.* **1995**, *117*, 5614–5615. (b) Matyjaszewski, K.; Xia, J. *Chem. Rev.* **2001**, *101*, 2921–2990. (c) Tsarevsky, N. V.; Matyjaszewski, K. *Chem. Rev.* **2007**, *107*, 2270–2299. (d) Matyjaszewski, K.; Tsarevsky, N. V. *Nature Chem.* **2009**, *1*, 276–288. (e) Braunecker, W. A.; Matyjaszewski, K. *Prog. Polym. Sci.* **2007**, *32*, 93–146.
- (56) Oh, J. K.; Drumright, R.; Siegwart, D. J.; Matyjaszewski, K. *Prog. Polym. Sci.* **2008**, *33*, 448–477.
- (57) Oh, J. K.; Tang, C. B.; Gao, H. F.; Tsarevsky, N. V.; Matyjaszewski, K. *J. Am. Chem. Soc.* **2006**, *128*, 5578–5584.
- (58) (a) Jakubowski, W.; Matyjaszewski, K. *Macromolecules* **2005**, *38*, 4139–4146. (b) Min, K.; Gao, H.; Matyjaszewski, K. *J. Am. Chem. Soc.* **2005**, *127*, 3825–3830. (c) Jakubowski, W.; Matyjaszewski, K. *Angew. Chem.* **2006**, *45*, 4482–4486. (d) Jakubowski, W.; Min, K.; Matyjaszewski, K. *Macromolecules* **2006**, *39*, 39–45.
- (59) Oh, J. K.; Siegwart, D. J.; Lee, H. I.; Sherwood, G.; Peteanu, L.; Hollinger, J. O.; Kataoka, K.; Matyjaszewski, K. *J. Am. Chem. Soc.* **2007**, *129*, 5939–5945.
- (60) Oh, J. K.; Siegwart, D. J.; Matyjaszewski, K. *Biomacromolecules* **2007**, *8*, 3326–3331.
- (61) Bencherif, S. A.; Sheehan, J. A.; Hollinger, J. O.; Walker, L. M.; Matyjaszewski, K.; Washburn, N. R. *J. Biomed. Mater. Res., Part A* **2008**, *90A*, 142–153.
- (62) Bencherif, S. A.; Sheehan, J. A.; Srinivasan, A.; Walker, L. M.; Gayathri, C.; Gil, R.; Hollinger, J. O.; Matyjaszewski, K.; Washburn, N. R. *Acta Biomater.* **2009**, *5*, 1872–1883.
- (63) Shim, S. E.; Oh, S.; Chang, Y. H.; Jin, M. J.; Choe, S. *Polymer* **2004**, *45*, 4731–4739.
- (64) Tsarevsky, N. V.; Matyjaszewski, K. *Macromolecules* **2005**, *38*, 3087–3092.
- (65) Kim, K. H.; Kim, J.; Jo, W. H. *Polymer* **2005**, *46*, 2836–2840.
- (66) Oh, J. K.; Matyjaszewski, K. *J. Polym. Sci., Part A: Polym. Chem.* **2006**, *44*, 3787–3796.
- (67) Brannon-Peppas, L. *J. Controlled Release* **2000**, *66*, 321.
- (68) Siegwart, D. J.; Oh, J. K.; Gao, H. F.; Bencherif, S. A.; Perineau, F.; Bohaty, A. K.; Hollinger, J. O.; Matyjaszewski, K. *Macromol. Chem. Phys.* **2008**, *209*, 2180–2193.
- (69) Hong, P. D.; Chen, J. H. *Polymer* **1998**, *39*, 5809–5817.

BM9004639